Functional Materials

DOI: 10.1002/anie.201300856

Hybrid Nanoscale Organic Molecular Crystals Assembly as a Photon-Controlled Actuator**

*Tian Lan and Wei Chen**

Micro- and nanoscale machines and robots with simple structures that can directly transform environmental energy into mechanical work are in high demand. Traditional electromotors usually have the inductor, controller, generator, motor, and transmission integrated into one system. Until now, a variety of energy forms, including electricity, heat, light, and ion transfer, have been widely applied to drive actuators.[1–4]

Among these energy forms, light is a multiparameter-adjustable stimulus, that is, the monochromaticity, wavelength, intensity, polarization, and the position of illumination can be precisely tuned to manipulate the actuator.[5–7] In addition, unlike for other stimuli, light parameters can be controlled remotely without the need for direct contact with the actuator, thus making it possible to simplify the device by getting rid of complex components, reducing the size and weight, and minimizing the structure in a freestanding configuration.

Photoisomers have been used in several types of photoresponsive actuators, for example, azobenzene in liquid crystal elastomers (LCEs), and diarylethene and anthracene derivatives in microscale molecular crystals. In LCEs, the driving force is the phase inversion caused by photoisomerization of azobenzene mesogens.[8] LCE actuators have high frequency oscillation, wavelength selectivity, and polarization selectivity and significant properties derived from large strain and stress.[7,9,10] The grafting of azobenzene moieties onto a polymer skeleton should change the intrinsic properties of a material, however, the phase inversion process usually takes a relatively long time to cause deformation of the whole LCE. In comparison with LCEs, molecular crystals can be actuated directly as a result of photoisomerization and subsequent lattice deformation of dye molecules, thus presenting much better repeatability, fatigue resistance, and faster response rates. Nevertheless, molecular crystal actuators are fragile and are highly restricted in performance by the crystal size and shape.[11–18] Macroscale molecular crystals rarely present ideal deformation properties and it is still a challenge to use molecular crystals in macroscale actuators.

Herein, we report the development of a hybrid nanoscale organic molecular crystal assembly as a photoresponsive actuator. In this novel system, rod-like nanocrystals of 2-hydroxynaphthylidene-1′-naphthylamine (HNAN) are selectively oriented and unevenly distributed in a compact polyvinylidene fluoride–hexafluoropropylene (PVDF–HFP) copolymer membrane. Compared with pure PVDF–HFP, which does not show any response to UV light, the composite membrane presents UV-induced bending, even with only 1 wt% of HNAN. Such an assembly approach would be a practicable way to combines the advantages of both LCEs and molecular crystals for actuator design.

HNAN is synthesized by a previously reported method.[19] This kind of Schiff base molecule will undergo isomerization after being exposed to UV light of the appropriate wavelength, and recover its initial state when the UV light is turned off. In our experiment, HNAN (2 mg) and PVDF–HFP (200 mg) are dissolved in DMF (2 mL) to form a homogeneous viscous solution. After being cast onto a 75 mm × 25 mm glass slide, the mixture is heated at 80 °C until the DMF is completely evaporated, to leave a yellow, transparent composite membrane approximately 52 μm in thickness.

An SEM image of a section of the membrane (Figure 1a) shows that the hybrid structure mainly consists of rod-like nanoparticles that are embedded in a multilayer polymer matrix. The length and aspect ratios of these nanorods vary from 300 nm to 900 nm, and 4 to 5, respectively. In the DMF solution HNAN tends to form large rod-like crystals, whereas in the viscous polymer solution HNAN tends to form nanorods because of the low molecular diffusion and low rate of crystallization. These nanorods are in a gradient distribution and generally oriented parallel to the membrane surface (Figure 1b). XRD patterns of pure PVDF–HFP, HNAN powder, and a horizontally placed composite membrane are shown in Figure 1c. In the XRD pattern of HNAN, the strongest peaks at $2\theta = 10°$, 12°, and 26° correspond to the (100), $(10\bar{2})$, and (210) crystal faces of HNAN, respectively. In the XRD pattern of the composite membrane, in addition to the characteristic peaks for PVDF–HFP, only the peaks at 12° and 26° are present, thus indicating that a low amount, decreased particle size, and orientated distribution of HNAN

[*] T. Lan, Prof. W. Chen
i-Lab, Suzhou Institute of Nano-Tech and Nano-Bionics
Chinese Academy of Sciences
Suzhou 215123 (P.R. China)
E-mail: wchen2006@sinano.ac.cn
T. Lan
University of Chinese Academy of Sciences
Beijing 100049 (P.R. China)
and
Institute of Chemistry, Chinese Academy of Sciences
Beijing 100101 (P.R. China)

[**] We acknowledge the Natural Science Foundation for Distinguished Young Scientists of Jiangsu Province (BK2012008), the Hong Kong, Macao and Taiwan Science & Technology Cooperation Program of China (2012DFH50120), the National Natural Science Foundation of China (21143004, 11204350), the National Basic Research Program of China (2010CB934700), and the Natural Science Foundation of Jiangsu Province (BK2011365).

Supporting information for this article is available on the WWW under http://dx.doi.org/10.1002/anie.201300856.

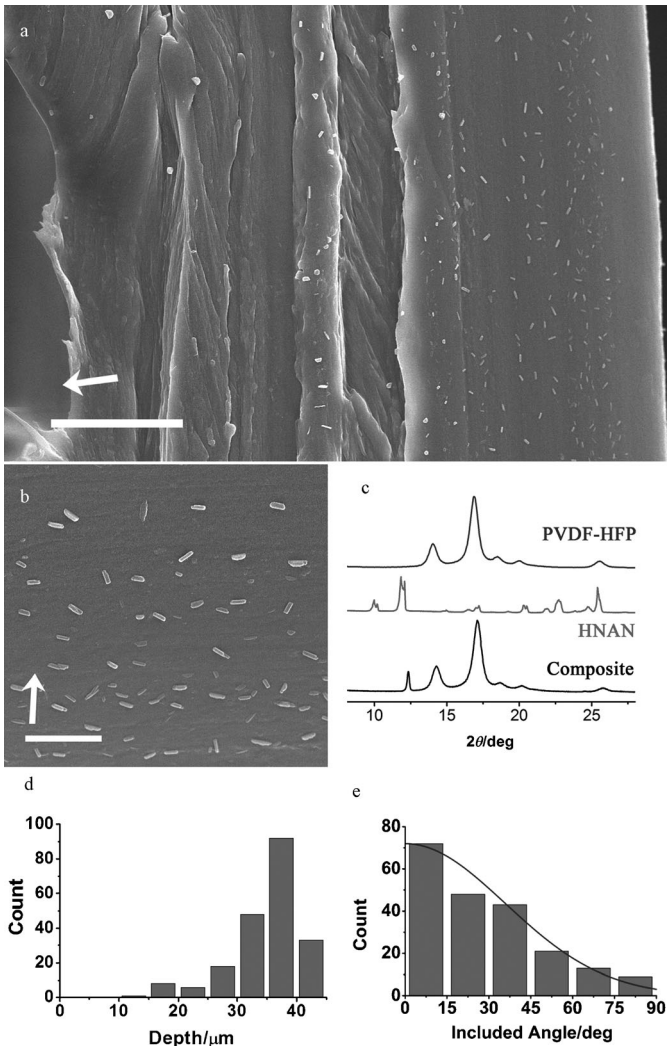

Figure 1. a) SEM image of composite membrane section showing gradient distribution of nanorods; scale bar: 10 μm. b) Amplified region of the SEM image of the composite membrane, showing the trend for the orientation of the nanorods parallel to membrane surface; scale bar: 2 μm. c) XRD patterns of PVDF–HFP, HNAN powder, and composite membrane. d) Gradient distribution statistics of the nanorods. e) Orientation statistics of the nanorods. The arrows in a) and b) perpendicularly point to the upper surface of membrane when casting.

nanorods would lead to weakening and disappearance of the XRD peaks.

The nanorods are distributed unevenly in this system; the SEM image (Figure 1a) reveals that there are almost no nanorods near the upper surface, whereas there are many near the lower surface. Figure 1d shows the statistical positions of the nanorods in a randomly chosen region of the membrane, thus revealing the gradient distribution. The distribution density increases monotonically from the top to the bottom except for in an approximately 5 μm thick layer at the bottom of the membrane. In Figure 1e, nanorods in the same region are counted according to the included angle between their long axis and membrane surface, showing a selective orientation close to a normal distribution (see the Supporting Information, Figure S1). The degree of orientation is calculated to be 0.30.

For testing the photon-controlled actuation, the membrane is cut into pieces 25 mm × 2 mm in size and around 4.1 mg in weight, and one side is fixed to form a cantilever. A laser displacement sensor is used to detect movement of the free end of the sample, and a UV LED lamp is placed approximately 5 mm above the sample, to provide the UV light (365 nm in wavelength) at a power density of 24 mW cm^{-2} (Figure 2a). A cycle of UV illumination for

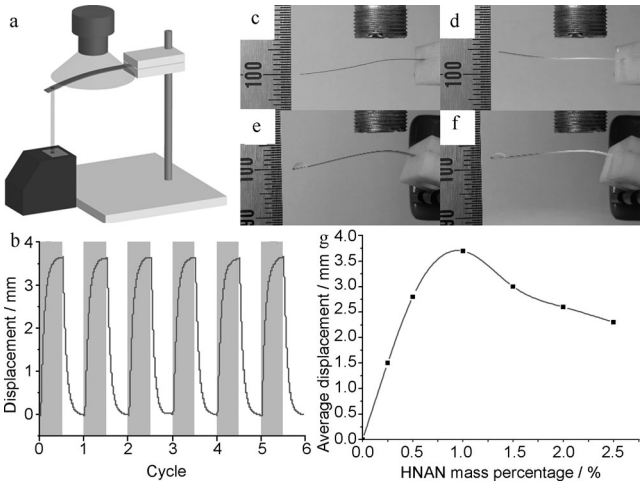

Figure 2. Actuation performance of composite membrane: a) Schematic representation of the testing method. b) Cyclic actuation displacement testing under UV illumination (gray). c) Photograph of membrane before UV illumination. d) Photograph of membrane after UV illumination. e) Photograph of membrane with 5 mg water on the top. f) Photograph of bending behaviour after UV illumination. g) Plot of actuation displacement against HNAN mass percentage.

15 seconds and then darkness for 15 seconds is repeated to stimulate the sample. The cantilever exhibits reversible bending and unbending behavior with an average displacement of about 3.7 mm (Figure 2b). The observed displacement is even larger (about 4.5 mm measured from Figure 2c and d). We attribute this difference to the fact that the laser displacement sensor cannot be precisely fixed at the top of cantilever. Even when a drop of water (5 μL, around 5 mg), which is 1.2 times of the weight of the cantilever (2.4 times of resisting moment), is placed on top of the cantilever, it is still lifted about 2.5 mm (Figure 2e and f). The robustness of the photoresponsive actuation is verified by performing 50 continuous cycles and by testing after 4 months (see the Supporting Information, Figure S2 and S3). To study the relationship between actuation performance and composition of the membrane, samples with different amounts of HNAN from 0.25 wt% to 2.5 wt% are measured (see the Supporting Information, Figure S4). The average displacement detected by the laser sensor increases initially with the content of HNAN, reaches the maximum for the sample with 1.0 wt%, and then decreases slowly (Figure 2g).

Almost 90% amplitude of displacement can be reached in 6 seconds under UV illumination (Figure 2b). Although the

strain rate of HNAN composite is slower than that of reported LCEs and HNAN single crystals, the molecular crystal assembly is relatively larger and requires a much weaker UV illumination (less than the reported intensity by about 1–2 orders of magnitude).[20,21] Usually, the size of the sample and UV intensity affect the strain and strain rate considerably. For the nanoscale molecular crystal assembly, the photon-controlled actuation is also greatly dependent on the microstructure of HNAN in composite, see below.

Interestingly, no matter which surface is illuminated, the membrane always bends towards the lower surface, in which there is a higher density of nanorods. Variation of the temperature of the membrane during UV illumination is measured to be within 2 °C, which is too small to cause the visible bending motion (see the Supporting Information, Figure S5 and S6). The upper layer can be considered as pure polymer, which has no response to UV light. All these phenomena indicate that the bending is definitely caused by the embedded HNAN nanorods in the lower layer. The intrinsic asymmetry is quite different from that of LCEs whose asymmetry only occurs when they are illuminated. We believe the gradient distribution and orientation plays a critical role in the bending process.

Figure 3 shows the formation of HNAN nanorods with gradient distribution and orientation, and the deformation mechanism of the composite membrane. When the homogeneous solution of HNAN and PVDF–HFP in DMF (Figure 3a) is heated, DMF evaporates, resulting in polymer solidification at the gas–liquid interface and HNAN crystallization in the interior. However, the solidification and crystallization cannot take place synchronously because the initial solution is not saturated with HNAN. Therefore, the upper solidified layers contain few nanorods and can be considered as pure PVDF–HFP. The crystallization of HNAN increases with further evaporation of solvent, and thus the number of the HNAN nanorods increases from top to the bottom, presenting a gradient distribution as illustrated in Figure 1b.

The polymer undergoes dissolution, swelling, and solidification in sequence during membrane fabrication. The phase interfaces should be parallel to the membrane surface. Crystallized nanorods formed across such phase interfaces will definitely have higher surface free energy than those with parallel orientation. Therefore, the nanorods formed are initially randomly oriented (Figure 3b′) but will orient horizontally to decrease the system energy (Figure 3c and c′). Such orientation will be further enhanced with shrinkage of the polymer matrix. The nanorods tend have a gradient distribution and be oriented parallel to the membrane surface, thus these HNAN composite membrane display photon-controlled actuation (Figure 3d). Owing to the polymer solidification, the fixed nanorods are stable and retain such distribution and orientation even after UV illumination.

To understand the deformation mechanism of the nanoscale molecular crystal assembly, a single HNAN crystal was formed by the solvent evaporation method in pure DMF and subjected to the same UV illumination (Figure 4a). A reversible actuation displacement of about 2 μm in 32 ms (Figure 4b and Figure S7) is detected for the microscale rod-

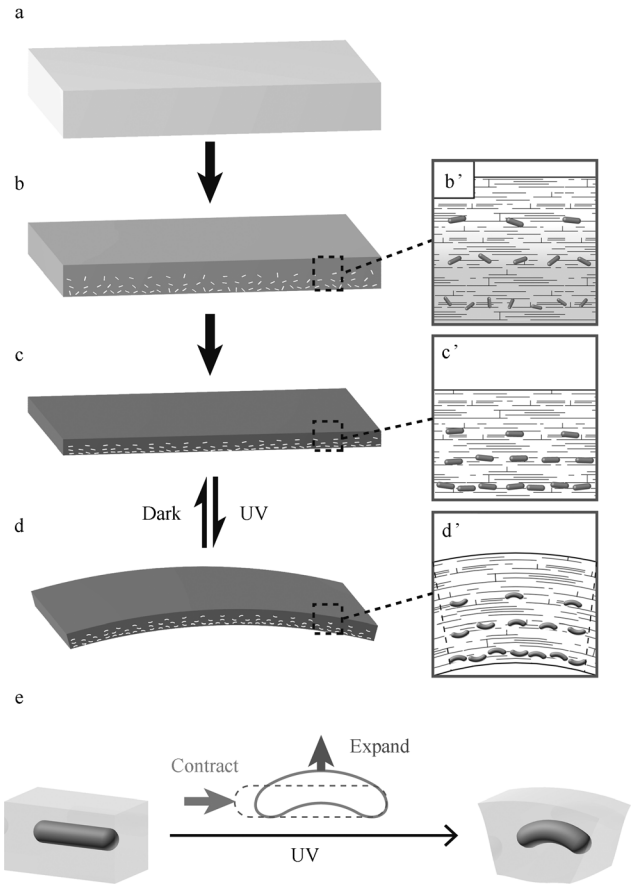

Figure 3. Mechanism of distribution, orientation, and bending: a) Homogeneous solution. b) Polymer solidification and crystallization of HNAN into nanorods with gradient distribution during evaporation. b′) Random orientation of HNAN nanorods in polymer matrix. c) Orientation of nanorods parallel to membrane surface. c′) Nanorods oriented along phase interfaces. d) Deformation of the whole composite membrane under UV illumination. d′) Deformation of all nanorods in lower layer induces contraction of polymer matrix. e) Contraction in horizontal direction and expansion in vertical direction for one nanorod and the surrounding polymer.

like sample 10.0 mm × 0.5 mm × 0.3 mm in size. In principle, a Schiff base undergoes photoisomerization and photochromism, including proton transfer and bond rotation, under UV illumination.[22] A change in the included angle between two naphthaline molecules can induce a deformation of the crystal

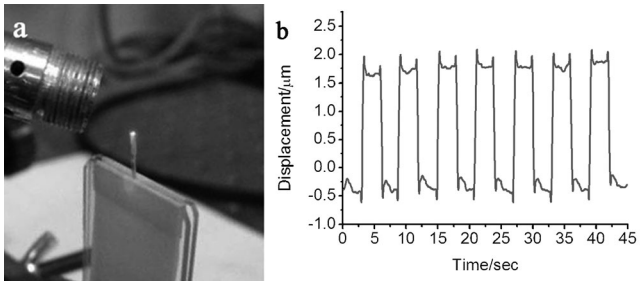

Figure 4. a) HNAN macroscale single crystal and b) its reversible bending detected by a laser displacement sensor under 365 nm UV illumination.

lattice and subsequent deformation of the whole molecular crystal. For smaller crystals, the crystal deformation will be further enhanced owing to the high surface-to-volume ratio providing sufficient strain relief.[23]

The deformation mechanism shown in Figure 3e is proposed for the assembly of HNAN nanoscale crystals in polymer. Under UV illumination, horizontally placed nanorods will bend to give an arched shape; these bent rods occupy a larger vertical space and smaller horizontal space than that of unbent nanorods. Such deformation will consequently drive the surrounding polymer unit to contract in the horizontal direction and expand in the vertical direction. As mentioned above, the orientation of the nanorods are mostly influenced by the phase interfaces, and their long axes tend to be parallel to the membrane surface. Thus local contraction will affect the parallel layers, and local expansion will affect the thickness. Based on these findings, it is reasonable to consider that such deformation could be more apparent with more nanorods embedded. However, it has been verified in our experiment that increasing the amount of HNAN nanorods results in the loss of another important factor for the deformation, that is, the gradient distribution of the nanorods. With the gradient distribution, the contraction will increase monotonically from top to the bottom of membrane. The lower surface of membrane will undergo a stronger contraction than the upper layer as seen in Figure 3d′. After the UV stimulus is removed, the nanorods recover, as well as the surrounding polymer and the whole membrane. Therefore, the influence of the number of nanorods and together with that of the gradient distribution explains the influence of the mass percentage of the nanorods on the actuation performance, shown in Figure 2g. The amount of nanorods will change the distribution as well as density of energy conversion units. If there are too few nanorods more UV power will be required, whereas too many nanorods will lead to a loss in the gradient distribution, thus, the optimal mass percentage of nanorods at around 1.0 wt%. Compared with other anisotropic nanocomposite systems, in which the orientation of nanorods is often achieved through mechanical stretching, the introduced approach involving phase-interface-induced self-assembly undoubtedly ensures the compactness and mechanical strength of the polymer matrix, both of which are beneficial to cyclic deformation and stable actuation. As well as the influence from HNAN nanorods, the intrinsic properties of the polymer were also taken into account. The PVDF–HFP matrix was replaced with polydimethylsiloxane and polystyrene, respectively, but the system of PVDF–HFP with HNAN nanorods provides the best actuation performance. Further studies aimed at probing the nature of correlation between polymer conformation and HNAN nanorods are underway.

In summary, we have described the photomechanical properties of a hybrid HNAN nanoscale molecular crystal assembly. The composite membrane undergoes deformation under relatively low-intensity UV illumination. A polymer containing HNAN nanorods with gradient distribution and orientation within a polymer was synthesized by a novel and simple method. The embedded HNAN nanorods work as high efficient energy conversion units, and the compact PVDF–HFP matrix is the supporting exoskeleton, which successfully transmits and accumulates inner stress and strain of each unit to a macroscale membrane. By these characteristics, the novel structure can be considered as a bridge between molecular crystals and liquid crystal elastomers. We hope to further combine the respective advantages of molecular crystals and liquid crystal elastomers and develop more efficient photon-controlled actuators.

Experimental Section

Materials: 2-Hydroxyl-1-naphthaldehyde and 1-naphthylamine are purchased from Alfa Aesar, PVDF-HFP is purchased from Sigma–Aldrich Chemical Co., LLC, and DMF is purchased from Sinopharm Chemical Reagent Co., Ltd. All the reagents are used as received.

Synthesis of 2-hydroxynaphthylidene-1′-naphthylamine (HNAN): A solution of 2-hydroxyl-1-naphthaldehyde (2.5 mmol) and 1-naphthylamine (2.5 mmol) in ethanol (20 mL) was heated to reflux. The mixture was stirred for 5 h until no more orange precipitate generated. The ethanol was then removed and the crystalline precipitate was dried. The obtained NHNA was used without further purification.

Composite fabrication: PVDF–HFP (200 mg), NHNA (2 mg), and DMF (2 mL) were mixed and heated to 80 °C overnight to obtain a uniform solution. The mixture was then put onto a 75 mm × 25 mm glass slide, and heated at 80 °C until the DMF solvent had completely evaporated. The resulting HNAN/PVDF–HFP composite membrane was cut into pieces with appropriate size and shape for testing photon-controlled actuation. For reference, a pure PVDF–HFP membrane was fabricated by the same process.

Characterization: SEM observations were performed by Hitach S-4800. X-ray diffraction (XRD) measurements were recorded with D8-discover Bruker X-ray diffractometer with Cu Kα radiation ($\lambda =$ 1.5418 Å). Photon-controlled actuation was recorded by Keyence LK-G800 laser positioning system. Temperature was measured by using Fluke 59 mini IR thermometer.

Received: January 31, 2013
Revised: March 19, 2013
Published online: May 6, 2013

Keywords: hybrid materials · isomerization · materials science · nanoscale molecular crystals · photon-controlled actuator

[1] L. Lu, W. Chen, *Adv. Mater.* **2010**, *22*, 3745 – 3748.
[2] Y. Hu, W. Chen, L. H. Lu, J. H. Liu, C. R. Chang, *ACS Nano* **2010**, *4*, 3498 – 3502.
[3] T. Ikeda, J.-i. Mamiya, Y. Yu, *Angew. Chem.* **2007**, *119*, 512 – 535; *Angew. Chem. Int. Ed.* **2007**, *46*, 506 – 528.
[4] L. H. Lu, W. Chen, *Nanoscale* **2011**, *3*, 2412 – 2420.
[5] C. L. van Oosten, C. W. M. Bastiaansen, D. J. Broer, *Nat. Mater.* **2009**, *8*, 677 – 682.
[6] F. Terao, M. Morimoto, M. Irie, *Angew. Chem.* **2012**, *124*, 925 – 928; *Angew. Chem. Int. Ed.* **2012**, *51*, 901 – 904.
[7] Y. L. Yu, M. Nakano, T. Ikeda, *Nature* **2003**, *425*, 145 – 145.
[8] M. Kondo, Y. L. Yu, T. Ikeda, *Angew. Chem.* **2006**, *118*, 1406 – 1410; *Angew. Chem. Int. Ed.* **2006**, *45*, 1378 – 1382.
[9] T. J. White, N. V. Tabiryan, S. V. Serak, U. A. Hrozhyk, V. P. Tondiglia, H. Koerner, R. A. Vaia, T. J. Bunning, *Soft Matter* **2008**, *4*, 1796 – 1798.
[10] W. Wu, L. M. Yao, T. S. Yang, R. Y. Yin, F. Y. Li, Y. L. Yu, *J. Am. Chem. Soc.* **2011**, *133*, 15810 – 15813.
[11] S. Kobatake, S. Takami, H. Muto, T. Ishikawa, M. Irie, *Nature* **2007**, *446*, 778 – 781.

[12] M. Morimoto, M. Irie, *J. Am. Chem. Soc.* **2010**, *132*, 14172 – 14178.
[13] L. Zhu, R. O. Al-Kaysi, C. J. Bardeen, *J. Am. Chem. Soc.* **2011**, *133*, 12569 – 12575.
[14] L. Zhu, R. O. Al-Kaysi, R. J. Dillon, F. S. Tham, C. J. Bardeen, *Cryst. Growth Des.* **2011**, *11*, 4975 – 4983.
[15] H. Koshima, N. Ojima, H. Uchimoto, *J. Am. Chem. Soc.* **2009**, *131*, 6890 – 6891.
[16] H. Koshima, N. Ojima, *Dyes Pigm.* **2012**, *92*, 798 – 801.
[17] H. Koshima, K. Takechi, H. Uchimoto, M. Shiro, D. Hashizume, *Chem. Commun.* **2011**, *47*, 11423 – 11425.
[18] H. Koshima, H. Nakaya, H. Uchimoto, N. Ojima, *Chem. Lett.* **2012**, *41*, 107 – 109.
[19] M. Gavranić, B. Kaitner, E. Meštrović, *J. Chem. Crystallogr.* **1996**, *26*, 23 – 28.
[20] Y. L. Yu, T. Maeda, J. Mamiya, T. Ikeda, *Angew. Chem.* **2007**, *119*, 899 – 901; *Angew. Chem. Int. Ed.* **2007**, *46*, 881 – 883.
[21] K. M. Lee, M. L. Smith, H. Koerner, N. Tabiryan, R. A. Vaia, T. J. Bunning, T. J. White, *Adv. Funct. Mater.* **2011**, *21*, 2913 – 2918.
[22] K. Amimoto, T. Kawato, *J. Photochem. Photobiol. C* **2005**, *6*, 207 – 226.
[23] R. O. Al-Kaysi, C. J. Bardeen, *Adv. Mater.* **2007**, *19*, 1276 – 1280.

